X-ray diffraction from amorphous Ge/Si Cantor superlattices

K. Järrendahl, M. Dulea,* J. Birch, and J.-E. Sundgren
Department of Physics, Thin Film Physics Division, Linköping University, S-581 83 Linköping, Sweden
(Received 22 September 1994)

X-ray measurements on Cantor superlattices are reported. Indexing and scaling laws are derived for the distribution of peaks in the diffraction spectra of perfect superlattices. The peaks are indexed by three indices and the largest scaling exponents of the intensities are proportional to the fractal dimensions of the Cantor sets. The theoretical indexing scheme of the peaks is confirmed by experiment. The influence of the absorption and sample imperfections on the scaling of the peaks is investigated by means of numerical simulations. A discussion of the nature of the diffraction spectra in the thermodynamic limit is also included.

I. INTRODUCTION

There is a growing interest in the study of systems with long-range order like quasicrystals,[1] fractals,[2] and aperiodic superlattices.[3–5] Although not periodic, these structures are still deterministic in the sense that they do not admit a stochastic description, and therefore, can be considered as intermediate between crystals and disordered systems. The investigation of quasicrystals and deterministic aperiodic superlattices has pointed out the necessity of alternative theoretical techniques for the description and understanding of their diffraction spectra.[6–9] In the case of the deterministic fractals the diffraction studies have been restricted until now to optical experiments[10] and numerical simulations.[2,11] This paper presents experimental and theoretical investigations of the x-ray diffraction from a class of fractal superlattices based on Cantor sets.

The diffractograms of the quasi-one-dimensional systems with aperiodic order investigated up to now are characterized by specifying (i) the structure of the set E of points in the reciprocal space that supports the distribution of intensity maxima, and (ii) the dependence of the intensity maxima on the system size. In the kinematic formalism, the intensity diffracted by a sample of length L reads

$$I_L(q)=|F_L(q)|^2 , \tag{1}$$

where q denotes the scattering vector and F_L the Fourier transform of the electron density. In general, it is assumed[7] that for large enough L the maxima scale with the length of the system following a power law $I_L(q)\propto L^{\alpha(q)}$, where the exponent $\alpha\leq 2$. Experiments and theoretical studies have shown that both the structure of the support E and the values taken by the exponent α strongly depend on the distribution of scatterers. Accordingly, there are three different types of spectra of finite-size one-dimensional systems.

(a) Spectra of Bragg peaks for which there is an indexation scheme and $\alpha=2$. Such spectra are, for instance, produced by periodic systems (where the set E is the reciprocal lattice), incommensurate systems and the Fibonacci superlattice.[3]

(b) Diffuse spectra, in which no indexation of the peaks is possible and the mean scaling exponent of the intensity maxima is $\alpha=1$. The classical example of diffuse spectrum is that of the amorphous solid, but one-dimensional aperiodically ordered systems with spectra of the same type are also known (e.g., the Rudin-Shapiro chain[12]).

(c) Spectra composed of peaks which are not Bragg peaks ($\alpha<2$) and for which indexation rules exist, like the spectrum of the Thue-Morse system.[5,13]

It should be noted the role played by the large-system limit process in the characterization of the spectra mentioned above. In case (b) the number of peaks increase and their location changes with L, such that a simple description of the support E is possible only in the thermodynamic limit (when E becomes an interval). On the other hand, an increase in the number of the unit cells does not affect the structure of the set E in periodic systems. Most of the spectra of the investigated deterministic aperiodic systems exhibit a behavior in between the two limit cases above, that is, additional peaks are generated when L grows but their location is stable and governed by some indexation rules. Therefore, it is expected that the study of the nature of spectra of these systems in the limit of the infinite size will lead to qualitatively different results.

A convenient description of the diffraction spectra in the thermodynamic limit can be made in terms of the *integrated intensity,* which is defined by

$$H(q)=\lim_{L\to\infty}\int_0^q \frac{I_L(q')}{L}dq' , \tag{2}$$

and represents the (normalized) distribution of the diffracted intensity registered up to some point q in the reciprocal space.[14] The function H is an indicator of the type of diffraction spectrum. If the system is periodic there are intervals on the q axis, where $I_L(q)=0$ and which give no contribution to the integrated intensity, that is on which $H(q)$ is constant. These intervals are separated by the points of the reciprocal lattice where the Bragg peaks are located and where $H(q)$ has finite jumps. More generally, the integrated intensity of any system of type (a) is discontinuous and the set E of its discontinuities is at most countable. This can formally be written,

 ©1995 The American Physical Society

$$H(q)=\int_0^q \sum_\nu c_\nu \delta(q'-q_\nu)dq' \ , \tag{3}$$

where the sum runs over some countable set of values, δ denotes the Dirac's generalized function, and the coefficients $c_\nu > 0$.

On the contrary, if the spectrum is diffuse then the contribution to H of any interval on the q axis is roughly proportional to its length. By making these intervals arbitrarily small it can be seen that $H(q)$ is continuous and derivable, and then a positive function F exists such that

$$H(q)=\int_0^q F(q')dq' \ . \tag{4}$$

It is more difficult to describe the function H in case (c). It is generally expected that in the infinite limit the diffraction maxima are more agglomerated than the peaks are in case (a) but their support E is still very thin. The function H is continuous, but the contribution of any interval to H is not simply related to its length. The set E is no longer composed of intervals and/or a countable set of points as in the cases (a) or (b) above and its structure is similar to that of a Cantor set, which is described in Sec. II. In this case a finer characterization of the diffraction pattern is required, which allows us to quantize how much of the spectrum is supported by *any* set of geometric points on the q axis.

A unified description of the spectrum which places the tree cases above on the same footing can be made in terms of the *intensity measure,* which is a non-negative function of sets defined by

$$H(q)=\int_0^q d\mu(q') \ . \tag{5}$$

The measure μ attaches to any set of points on the q axis a weight proportional to the diffracted intensity registered at these points. The intensity measures corresponding to the cases (a) and (b) are qualitatively different. In case (a) the weight of any set in the reciprocal space is equal to the sum of those coefficients c_ν from Eq. (3) for which the scattering vectors q_ν belong to the set. A measure with this property is said to be *discrete.*[15] In case (b) any single point in the spectrum has zero weight, while the weight of any finite interval from E is strictly positive. This is the definition of an *absolutely continuous* measure.[15]

The intensity measure is a good candidate for the description of the structural complexity, being discrete for strongly ordered systems (e.g., periodic) and absolutely continuous for (quasi-) random systems. It is natural to assume that some systems with degrees of order intermediate between periodic and random could be characterized by intensity measures which are neither discrete nor absolutely continuous. A measure of this type is called *singular continuous* (SC). By definition, a SC intensity measure describes a spectrum which does not contain δ peaks and whose support E is thin enough in the sense that it can be covered by a system of open intervals with arbitrary small total length.[15] It is widely believed that the intensity measures of many systems with exotic spectra of class (c) are SC but very few proofs of this kind are known.[7,16,17]

The study of the systems whose physical properties are described by SC measures has generated a considerable interest.[18] Recently, x-ray-diffraction experiments were performed on a GaAs/Al_xGa_{1-x}As heterostructure grown according to the Thue-Morse sequence whose intensity measure is SC.[5] Nevertheless, to the best of our knowledge, no experimental evidence of the features typical of SC measures has yet been found in diffractograms from fractal systems. This could be motivated, in the case of the two-component fractal systems like the Cantor superlattices, by the fact that the concentration of one of the components goes to zero in the thermodynamic limit such that the system looks uniformlike in a first approximation. Then the intensity measure is noninteresting, being dominated by a trivial Bragg peak generated by the majoritary component. However, here we prove that besides the Bragg peak there is a finer peak structure in the diffractograms which is exclusively due to the self-similar distribution of both components. Thus, the intensity measure as defined by Eqs. (2) and (5) does not satisfactorily reflect the effect the Cantor distributions of scatterers have on the diffraction spectra. Instead, the fine structure of the spectra is shown to be controlled by a different class of measures specific to these fractal systems, which are at least in one case singular continuous.

The outline of the paper is as follows. In Sec. II, the generation of the Cantor sets (and the idea of modulating superlattices according to them) is explained. In the next section, diffractograms from low-resolution x-ray-diffraction measurements and experimental details regarding the growth and the analysis of the superlattices are presented. The expressions for the positions and the scaling of the diffraction peaks are discussed in Sec. IV together with results from numerical reflectivity simulations of perfect Cantor superlattices. The derivation of the indexing and scaling expressions is exposed in Sec. V. In addition a measure-theoretical characterization of the Cantor spectra is made. Finally, in Sec. VI the theoretical results are compared with the data from detailed high-resolution x-ray-diffraction measurements.

II. CANTOR SUPERLATTICES

A Cantor set[19] is defined as what is left from a finite segment after removing parts of it according to some iterative procedure. For instance, the construction of the well-known triadic Cantor set (or "Cantor middle third" set) begins by taking a segment of unit length, dividing it in three equal parts and removing its middle third (without its endpoints). This results in the first-order approximant of the set, which contains two segments separated by a gap [Fig. 1(a)]. The middle third parts of the two segments from the first approximant are then removed, giving the second-order approximant, which is composed of four segments of length $\frac{1}{9}$ separated by the gap generated at the first step and two gaps of length $\frac{1}{9}$. By extrapolating this iterative procedure to infinity the triadic Cantor set is obtained, which is composed of geometric points distributed such that each point lies arbitrarily close of other points of the set. This set is self-similar and has the fractal dimension[19] $D_2=\ln(2)/\ln(3)$

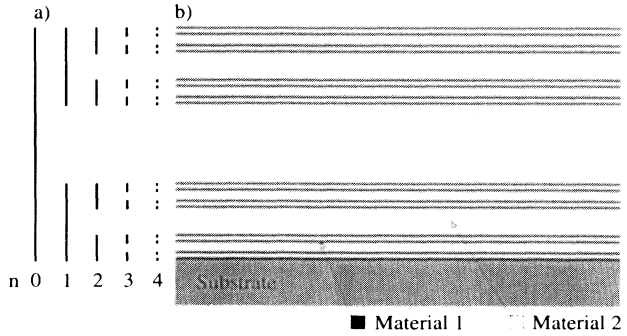

FIG. 1. (a) The first four generations leading to the Cantor middle third set ($r=2$). (b) A schematic drawing of a Cantor superlattice built according to the fourth generation of the Cantor middle third structure. The gaps and segments are represented by two different materials.

$=0.6309\ldots$.

Various Cantor sets can be generated by iterating the more general operation that consists in the division of a segment in $s=2r-1$ equal parts ($r=2,3,\ldots$) and the removal of $r-1$ of its pieces such that r disconnected segments and $r-1$ gaps are obtained. These sets are also self-similar and have the fractal dimensions,

$$D_r=\frac{\ln(r)}{\ln(s)} . \tag{6}$$

Figure 2(a) shows the generation of a Cantor set, here called the "Cantor double fifths" set, which corresponds to $r=3$. At every step each segment is divided in five parts of equal length. Two of these parts are then removed, leaving three disconnected segments with a length of one-fifth of the original segment. The continuation of this procedure gives a Cantor set with the fractal dimension $D_3=\ln(3)/\ln(5)=0.6826\ldots$.

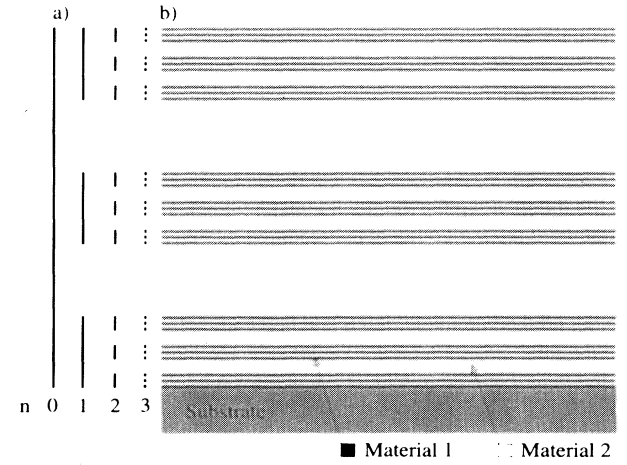

FIG. 2. (a) The first three generations leading to the Cantor double fifths set ($r=3$). (b) A schematic drawing of a Cantor superlattice built according to the third generation of the Cantor double fifths structure. The gaps and segments are represented by two different materials.

Superlattices can be grown by alternatively depositing two kinds of materials such that their distribution along the growth axis is identical to the distribution of segments and gaps in the finite order approximants of the Cantor sets. The thickness a of the layers which represent the segments should be large enough to give a significant scattering contribution and small enough to prevent excessive absorption in samples with many layers. For fixed a the thickness of each layer representing a gap is chosen to be a times the ratio between the length of the gap and the length of the segments (note that the lengths of the segments and of the smallest gaps are equal). In Figs. 1(b) and 2(b) the idea of building perfect superlattices according to the finite order approximants of the Cantor sets is presented.

The construction and the theoretical treatment of Cantor superlattices can be simplified if we observe that in any finite order approximant of a Cantor set the lengths of all gaps are integer multiples of the length of the smallest gap. The superlattice can then be seen as being obtained by deposing the two materials in layers of type A and B with the same thickness a which are distributed according to a well-defined aperiodic sequence. The segments correspond to single layers of type A, while the gaps correspond to clusters (i.e., finite sequences) of layers of type B. For instance, the sequence of layers corresponding to the second-order approximant of the triadic Cantor set reads $ABABBBABA$.

This approach identifies the growth of the Cantor superlattices with a process of inflation of the two types of layers A and B. Starting from a layer of type A the sequence of layers is generated by successively applying the concurrent substitution rules,

$$A\rightarrow ABA\ldots BA,\ B\rightarrow BB\ldots B , \tag{7}$$

where the right-hand side of the first and second substitution contains r A's and s B's, respectively. That is, at the first step the layer A (the "seed") is substituted by the multilayer $ABA\ldots BA$ (the first generation of the superlattice), which corresponds to the first-order approximant of the Cantor set. The second-order generation is obtained by substituting each A by $ABA\ldots BA$ and each B by $BB\ldots B$ in the first generation. In general, the physical realization of the nth order approximant of a Cantor set is the multilayer obtained from the seed A after applying the substitution rules (7) n times, and is called the nth generation of the Cantor superlattice. For instance, the first two generations of the sequence associated with the double fifths Cantor set ($r=3,s=5$) read $A\rightarrow ABABA\rightarrow ABABABBBBBABABABBBBBABABA$.

Similarly, if the substitution rules are applied to the seed B instead of A, a succession of growing clusters of B layers is obtained which describes the growth of the gaps in the approximants of the Cantor sets. The resulting "superlattice" of B layers is below called a B system and plays an important role in computing the Fourier transform of the Cantor superlattices.

The substitution rules (7) allow us the derivation of simple recurrence relations relating the thicknesses of the successive generations of each Cantor superlattice and its associated B system. They read

$$L_n = rL_{n-1} + (r-1)l_{n-1}, \quad l_n = sl_{n-1}, \quad L_0 = l_0 = a \ , \qquad (8)$$

where L_n and l_n denote the thickness of the nth generation of the Cantor superlattice and B system, respectively. According to Eq. (8) both systems grow like s^n.

III. EXPERIMENTS

Various Cantor superlattices were grown by dual target unbalanced dc magnetron sputtering at a base pressure below 1.3×10^{-5} Pa (1×10^{-7} Torr).[20,21] The A's and B's in the Cantor structures were represented with a nm of amorphous germanium (a-Ge) and a nm of amorphous silicon (a-Si), respectively, deposited onto Si(001) substrates with its native oxide. The sputtering of the Ge and Si layers was done using targets 50 mm in diameter with purities $>99.99\%$ in a high-purity Argon gas atmosphere at a pressure of 6.7×10^{-1} Pa (5×10^{-3} Torr). The target voltages were approximately 520 and 550 V and the target currents 40 and 140 mA for Ge and Si, respectively. This resulted in growth rates of approximately 0.1 nms^{-1} as measured with a dual-head quartz-crystal monitor. In order to obtain dense a-Ge and a-Si films at ambient substrate temperature, a negative substrate bias of 140 V was used during the depositions.[22,23] The modulation of the superlattices was achieved with the aid of two computer-controlled shutters in front of the Ge and Si targets. In the controlling software, the Cantor sequences, among many others, can be generated with r, s, and a as input parameters.

Cross-sectional transmission electron microscopy (XTEM) was used to confirm the grown sequences and to investigate the layer uniformity. These results showed that the layers were relatively sharp and that individual layers with thicknesses of less than 1.0 nm could be grown. In Fig. 3 an XTEM micrograph of a sample grown to the 6th generation of the Cantor middle third superlattice ($r=2$) is shown. The A's (the segments) and B's (forming the gaps) are represented here by layers of a-Ge and a-Si, respectively. In the image only the first 5 generations are resolved. Further information concerning the XTEM work can be found elsewhere.[20,22,23]

Low-resolution θ-2θ x-ray-diffraction (XRD) scans were performed on a conventional Philips powder diffractometer using Cu $K\alpha$ radiation. For more detailed θ-2θ XRD scans, using Cu $K\alpha_1$ radiation, a Philips Materials Research Diffractometer (MRS) equipped with a four-crystal high-resolution monochromator in the Ge-(220) setting and a $\frac{1}{4}$ degrees receiving slit was used. All the diffraction peaks from the superlattices were found at low scattering angles 2θ due to the amorphous structure in the layers. The low resolution and detailed measurements gave 2θ resolutions of 0.01° and better than 0.005°, respectively. Peak positions and intensities in the diffractograms were examined using the Philips *APD* software. The profile fit option in this software made it possible to also deconvolute peaks that were not well resolved in the diffractograms. The intensity in all experimental diffractograms was normalized to the intensity at the critical angle of the total external reflection I_0 near $2\theta=0.5°$.

Figure 4 shows a low-resolution diffractogram from the 6th generation of the Cantor middle third superlattice ($r=2$). The a-Ge and a-Si layer thicknesses were nominally $a=1.4$ nm. A low-resolution diffractogram from the 4th generation of the Cantor double fifths superlattice ($r=3$) with nominally $a=1.4$ nm is shown in Fig. 5.

An examination of the diffractograms shows that the peaks can be indexed with two integers (m,k) (the meaning of the values taken by m and k is explained in the next section). Both spectra display large oscillations in intensity, apparently irregular, but there are roughly similar groups of peaks, three carried by (1,1), (1,2), and

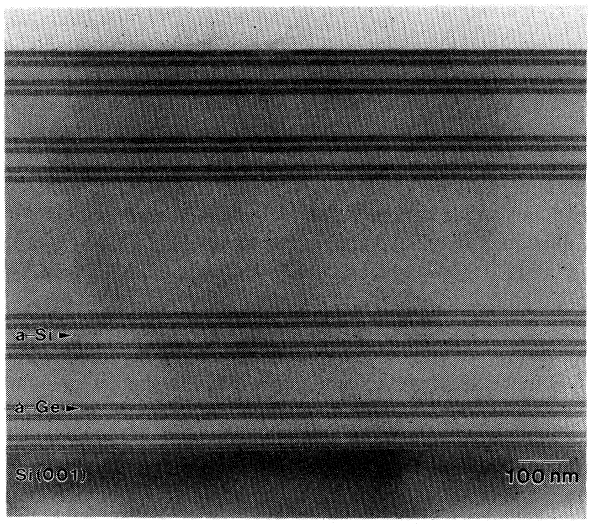

FIG. 3. An XTEM micrograph of the sixth generation of a Cantor middle third superlattice ($r=2$). The segments and gaps are represented here by layers of a-Ge and a-Si, respectively. In the image only the first five generations are resolved.

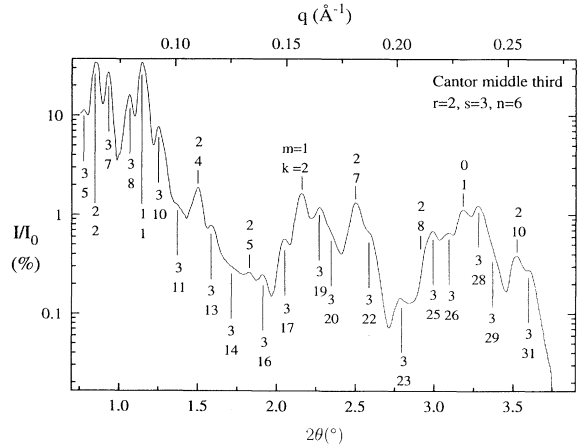

FIG. 4. Diffractogram from a low-resolution θ-2θ XRD measurement of the sixth generation of the Cantor middle third superlattice ($r=2$). The a-Ge and a-Si layer thicknesses were nominally $a=1.4$ nm. The 729 ($s^n=3^6$) A and B layers in the Cantor structure results in a total nominal thickness of 1020.6 nm.

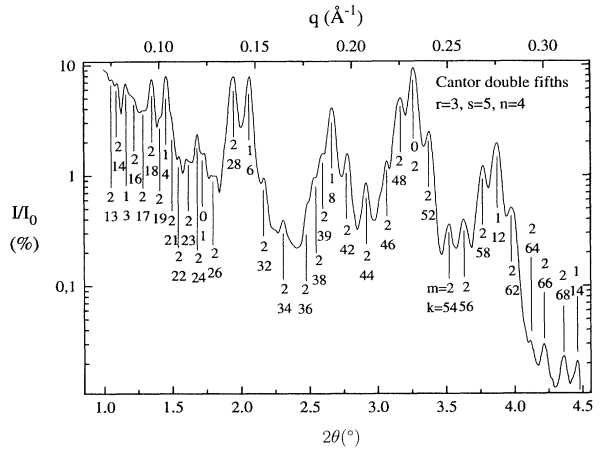

FIG. 5. Diffractogram from a low-resolution θ-2θ measurement on the fourth generation of the Cantor double fifths superlattice ($r=3$). The a-Ge and a-Si layer thicknesses were nominally $a=1.4$ nm. The 625 ($s^n=5^4$) A and B layers in the Cantor structure results in a total nominal thickness of 875 nm.

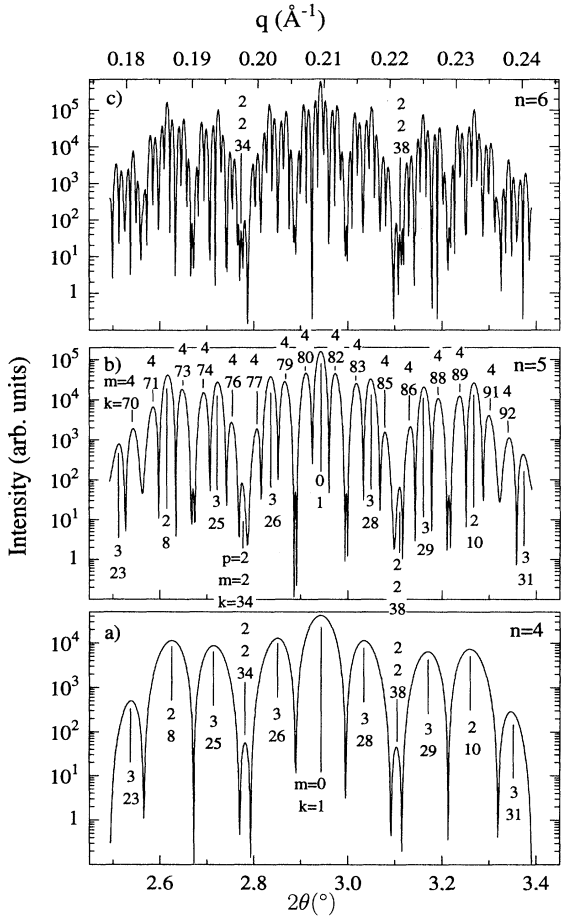

FIG. 6. Calculated diffractograms from the fourth (a), fifth (b), and sixth (c) generations of the Cantor middle third structure ($r=2$) with $a=1.5$ nm. From the figure it is clear that also the diffraction patterns of Cantor structures show self-similarity.

(0,1) in Fig. 4, and five around the peaks indexed with (1,4), (1,6), (1,8), (0,2), and (1,12) in Fig. 5. In general, a peak indexed with a given m dominates its neighboring peaks with larger m. Exceptions from this rule are the couples indexed with (0,1), (3,28), and (2,8), (3,25) in Fig. 4, and the couples indexed with (0,1), (2,24), and (1,14), (2,68) in Fig. 5. Also, there are weaker not indexed peaks in between the indexed ones, which appear sometimes as shoulders of the higher peaks. In Fig. 4, the index k takes all the values between the extrema except the multiples of three, while in Fig. 5 the multipliers of five are missing.

A complete analysis of the above results should take into account all the factors due to the sample imperfections or instrumental limitations, which can influence the location, intensity, and profile of peaks. In the next section, these factors are first neglected by performing a numerical simulation of the diffraction spectrum of a perfect sample. Then the alteration of the ideal diffractogram under the action of the above factor is discussed.

IV. NUMERICAL SIMULATIONS

Numerical computations of the scattering amplitude according to Eq. (1) were performed for perfect Cantor profiles characterized by uniform scattering densities inside the layers A and B, and sharp interfaces between the layers. In addition, more realistic x-ray reflectivity calculations were made using the Philips GIXA software in which a full dynamical theory is used taking care of multiple reflections, refraction and absorption.[24,25] The program contains a database with absorption data for x-ray energies between 0.1 and 100 KeV for most elements. Refractive index values are calculated from the atomic weight, density, and atomic number of the materials. The program can also make calculations based upon Fourier methods.

Figure 6 displays kinematically calculated diffractograms from the 4th, 5th, and 6th generations of the perfect Ge/Si Cantor middle third structure ($r=2$) with $a=1.5$ nm. The range of q values was chosen to correspond to the rightmost group of peaks in Fig. 4. (Identical results were obtained using the Fourier mode in the GIXA program.) From Fig. 6, it is clear that the diffraction patterns of Cantor structures exhibit self-similarity around the main peaks. When comparing the spectra produced by successive generations, a general feature is that all the peaks created by one generation survive and become stronger in the diffractogram of the next generation, with additional peaks appearing in between them. All the peaks indexed with $m \leq 3$ in Fig. 4 are already present in the simulated diffractogram of the 4th generation, and they grow and sharpen with increasing n. New, weaker peaks (indexed with $m=4$) appear at the 5th generation. This process continues at the 6th generation, producing an agglomeration of peaks that soon leads to a spacing between nearest-neighboring peaks which falls below the resolution power of the conventional x-ray-diffraction measurements. This explains why, even for perfect samples it is difficult to experimen-

TABLE I. The diffraction peaks can be indexed with more than one set of p, m, and k, according to Eq. (9). The table gives an example of how the indexing works in the Cantor middle third case ($r=2$) for $p=1$ peaks. The values of k in the same column correspond to the same peak. In this study all peaks have been indexed with the lowest possible p, m, and k, thus indicating their intensity behavior.

m	k																		
0										**1**									
1	**2**									3									**4**
2	6			**7**			**8**			9			**10**			**11**			12
3	18	**19**	**20**	21	**22**	**23**	24	**25**	**26**	27	**28**	**29**	30	**31**	**32**	33	**34**	**35**	36

tally resolve peaks with $m>4$. Some of the peaks with $m=4$ can still be identified as the nonindexed shoulders of the stronger peaks in Fig. 4 and are resolved in the detailed measurements treated in Sec. VI.

Figure 6 also shows, besides the peaks indexed with two integers, some weaker maxima indexed with three integers $p=2$, m, and k, in the neighborhoods of which the spectra are not self-similar. A theoretical investigation, to be presented in the next section locates all the peaks among the values of the scattering vectors given by

$$q(p,m,k)=\frac{2\pi}{a}\frac{k}{s^m(s^p-1)}\ , \tag{9}$$

where $p\geq 1$, $0\leq m\leq n-1$, and k takes any integer value. (When $p=1$, its value is not specified in diffractograms.) The intensities of the peaks indexed with $p=2$ in Fig. 6 are stationary (that is their heights do not grow with n), and their distribution is governed by simple quasiextinction rules to by derived in Sec. V. All the peaks are indexed with the lowest possible p, m, and k. (This explains why the multiples of three and five are absent in the values taken by k in Figs. 4 and 5, respectively.) An example is given in Table I of how the indexation works and how the peaks with different m and k are generated. The values of k in the same column correspond to the same peak.

As seen in Fig. 6, the peaks indexed with $p=1$ have the same rate of growth with n, while the intensity of the observed $p=2$ peaks is stationary. In Sec. V, it is shown that for large enough $n>m$ the intensity of the peaks indexed with (p,m,k) scales with the width L_n of the superlattice following the power law,

$$I_n(q)=C(r,m;q)L_{n-m}^{\alpha_r(k,p)},\quad n\gg m\ , \tag{10}$$

where the coefficient $C(r,m;q)$ does not depend on the generation number n, and $\alpha_r(k,p)\geq 0$. The maximum value of the scaling exponent $\alpha_r(k,p)$ is reached when $p=1$, and then it reads

$$\alpha_r(k,p=1)=2D_r\ . \tag{11}$$

Equation (11) directly relates the scaling of the diffraction peaks of the perfect Cantor superlattices to the fractal dimension D_r of the Cantor sets defined in Eq. (6).

The asymptotic expression (10) was tested by using the simulated intensity data for the triadic Cantor superlattice ($r=2$) from Fig. 6. Both Eqs. (10) and (11) were assumed to hold even for small $n>m$, but with the fractal dimension D_2 replaced by the approximants $D_2^{(n)}$, which can be computed from the ratios of the intensities of the same peak at two successive generations (I_n/I_{n-1}). In Table II it can be seen that the sequence of the approximants $D_2^{(n)}$ rapidly converges to the limit value $D_2=0.6309\ldots$ with increasing n, with a difference less than 1.1% at the 6th generation. Equation (10) was derived by assuming nonadsorbing layers. Data from a simulation in which absorption is taken into account are also included in Table II. In this case, the approximants $D_2^{(n)}$ start to decrease after a few generations, as expected. In conclusion, the absorption is expected to induce strong deviations from the scaling law Eq. (10) in the experimental diffractograms.

The intensity and the resolution of the diffraction peaks in a real superlattice are influenced by, for instance, instrumental limitations and sample imperfections such as layer thickness fluctuations, interface roughness (which give rise to a diffuse scattering[26]), and correlated roughness.[27] In the samples used in this work small layer thickness fluctuations and interface roughnesses are present, but no indications of correlated roughness have been observed by XTEM. To investigate the influence of the present imperfections, the diffraction from the 5th generation of a distorted Cantor middle third structure ($r=2$) was calculated. An offset in the deposition rates

TABLE II. The scaling of the diffraction peaks are directly related to the fractal dimension D_r of the Cantor sets according to Eqs. (10) and (11). For the Cantor middle third set ($r=2$), the fractal dimension is $D_2=0.6309\ldots$. From the intensity ratios of the same peak at two successive generations (I_n/I_{n-1}), approximants of the fractal dimension $D_2^{(n)}$ were calculated. The table shows data for the peaks with $(p,m,k)=(1,0,1)$ and $(1,0,3)$, in a Cantor middle third structure ($r=2$). The numerical calculations were made with and without absorption. In the case of no absorption the approximant $D_2^{(n)}$ rapidly converges to the limit value D_2, while the calculations with absorption shows that $D_2^{(n)}$ starts to decrease after a few generations.

	$D_2^{(n)}$		$D_2^{(n)}$ (absorption)	
n	(1,0,1)	(1,0,3)	(1,0,1)	(1,0,3)
2	0.3992...	0.5228...	0.3958...	0.5228...
3	0.5650...	0.5780...	0.5561...	0.5717...
4	0.6026...	0.6036...	0.5778...	0.5973...
5	0.6171...	0.6175...	0.5487...	0.5935...
6	0.6240...	0.6240...	0.4420...	0.5582...

was simulated by making the A layers (a-Ge) in the model 0.1 nm thinner and the B layers (a-Si) 0.03 nm thicker, such that the total thickness differed by less than 1% from the thickness in the perfect case. In addition, a Debye-Waller[28] interface roughness of 0.1 nm was introduced. The resulting diffraction pattern in Fig. 7 can be compared with the diffraction pattern from the corresponding perfect Cantor structure in Fig. 6(b). It is seen that while the peak positions are practically the same, the peak intensities are strongly influenced. Beside a general decrease in peak resolution it is observed that the peaks with smaller m can become dominated by some neighboring peaks with larger m, as, for instance, in the case of the couple (2,8), (3,25). This can explain the deviations seen in Figs. 4 and 5 from the general rule regarding the relative intensities of neighboring peaks which was stated in Sec. III. Other simulations in which the deposition rate offset was replaced with statistical errors of the layer thicknesses showed similar results.

V. THEORY

The theoretical model is a superlattice composed of layers of type A and B with thickness a arranged along the growth axis in a Cantor sequence. The distribution of the scattering density inside each layer is uniform. The interfaces are assumed perfectly sharp and the coordinate of the left end surface of layer j is denoted by z_j. The distribution of the scattering density is the convolution of the distribution of the electron density in the single layers A and B with the distribution of coordinates z_j (which is a sum of δ functions). Then the Fourier transform of generation n reads

$$F_n(q)=\sum_{j=0}^{s^n-1} e^{iqz_j} f_j(q) , \tag{12}$$

where $f_j(q)$ is the Fourier transform of layer j and takes

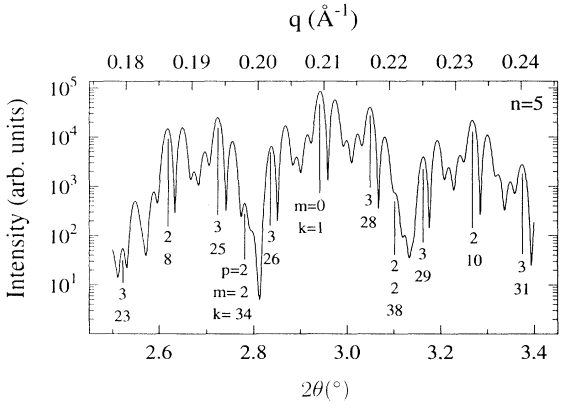

FIG. 7. Calculated diffractogram from the fifth generation of the Cantor middle third structure ($r=2$). The structure is distorted by making the A layers (a-Ge) 0.1 nm thinner and the B layers (a-Si) 0.03 nm thicker. In addition, a Debye-Waller interface roughness of 0.1 nm is introduced. The calculation should be compared with the corresponding perfect Cantor structure seen in Fig. 6(b). The peak positions are practically not affected, while the peak intensities are strongly influenced.

the values $f_A(q)$ or $f_B(q)$ if the layer j is of the type A or B, respectively.

According to the formalism outlined in the introduction, we are looking for values q_0 of the scattering vector for which, (i) $|F_n(q)|$ has a maximum at $q=q_0$ for any large enough n, and (ii) $|F_n(q_0)|$ grows with n as a power of L_n. In the theory of diffraction from crystals the intensity maxima (Bragg peaks) originate from the constructive interference of contributions coming from identical units (planes of atoms), which repeat periodically. Similarly, the intensity maxima of the Cantor superlattices are due to some clusters of layers that repeat along the growth axis.

The main maximum appears at $q=0$, when each layer A or B gives the same contribution to the Fourier transform. It is a Bragg peak which grows exponentially with n with a scaling exponent $\alpha=2$.

Other peaks with exponential growth appear from the contributions of clusters which repeat aperiodically. At each fixed generation n_0, the repeating clusters are all the previous generations with $n<n_0$, plus $r-1$ gaps. [This can be seen from the substitution rules (7), which define each $(n+1)$th generation as the union of r copies of the nth generation separated by the new gaps of the generation $n+1$.] Then the scattering amplitude F_{n+1} is the sum of the Fourier transforms of the copies of the nth generation multiplied by factors which describe their shift along the growth axis, plus the contribution of the gaps. This gives a system of coupled recurrence relations between the Fourier transforms of the successive generations of the Cantor superlattice and the B system (which describes the gaps). In a two-dimensional vectorial notation the recurrence relations read

$$\begin{bmatrix} F_{n+1}(q) \\ B_{n+1}(q) \end{bmatrix} = M(qL_n, ql_n) \begin{bmatrix} F_n(q) \\ B_n(q) \end{bmatrix} , \tag{13}$$

where B_n is the scattering amplitude of the nth generation of the B system. The matrix M of argument (x,y) reads

$$M(x,y)=\begin{bmatrix} S_r(x+y) & [S_r(x+y)-1]e^{-iy} \\ 0 & S_s(y) \end{bmatrix} , \tag{14}$$

where $S_r(t)$ denotes the trigonometric sum $\sum_{j=0}^{r-1} e^{ijt}$.

The above equations show that the contribution to F_{n+1} from the Fourier transforms F_n of the r copies of the previous generation is maximum when they are added (that is when the shift factor S_r reaches its maximum r). The same statement holds regarding the contribution to F_{n+1} coming from B_n (that is from the $r-1$ new gaps). To have a maximal exponential growth of $|F_n|$ with n the factor $S_r(qL_n+ql_n)$ should keep the same value r when n grows. Since the function $S_r(t)$ is periodic in t, the values of the argument $q(L_n+l_n)$ that correspond to different n should differ only by integer multiples of the period. The condition is trivially satisfied by the argument when $q=0$. Then the contribution to F_{n+1} coming from the gaps dominate [because $S_s(0)=s>r$] and $|F_n| \propto L_n$, giving the above-mentioned Bragg peak. (In fact in this case $e^{-iy}=1$, that is, F_n and B_n add in phase such that all lay-

ers give the same contribution, as expected.)

The case when the scattering amplitude is not dominated by the contribution of gaps is investigated below. The dependence of the argument of the matrix M on n is controlled by the recurrence relations (8) and can be written

$$U_{n+1}=M(0,0)U_n, \quad U_n=\begin{bmatrix} qL_n \\ ql_n \end{bmatrix}. \tag{15}$$

According to Eqs. (13) and (15) the variation of $|F_n(q)|$ with n for a fixed q value is governed by the product $P_n=M(U_{n-1})M(U_{n-2})\cdots M(U_0)$. As suggested above, steady growth with a maximal rate is possible when q takes such a value that the components of all the vectors U_j differ only by integer multiples k of the period 2π. This means that U_0 is a fixed point of the map (15) in which the variables are now considered as being defined modulo 2π in both components. Then the product matrix reads $P_n=[M(U_0)]^n$ and $|F_n|$ can grow exponentially with n with a constant rate if at least one eigenvalue of the matrix $M(U_0)$ has an absolute value greater than one.[9] A simple computation gives the values of the scattering vectors that correspond to the solution of the fixed-point equation $q=2k\pi/[a(s-1)]$, where k is an arbitrary integer.

The discussion above describes the case when each copy of the first generation along the chain gives the same contribution to the scattering amplitude of the generations $n>1$. The same reasoning can be applied to a situation when all the copies of the mth generation along the chain give identical contributions. Then the initial condition U_0 of the map (15) is such that the fixed point is reached at the mth iteration, and this happens when $q(k,m)=2k\pi/[a(s-1)s^m]$, where $m\geq 0$. When $m=m_0$ is fixed and k runs over the set of integers, $q(k,m)$ reproduces all the values corresponding to $m<m_0$ and arbitrary k, but new values appear each time when k is not a multiple of s^m ($m\leq m_0$). These new values of $q(k,m_0)$ correspond to the cases when the copies of the m_0th generation give identical contributions while the copies of the generations $n<m_0$ do not. Then the product matrix at any generation $n>m$ ($=m_0$) reads

$$P_n=[M(U_m)]^{n-m}M(U_{m-1})M(U_{m-2})\cdots M(U_0), \tag{16}$$

which means that steady growth with a constant rate could be reached beginning with the mth generation only. This explains why in diffractograms the peaks with smaller m are more intense than neighboring peaks with higher m values.

A further generalization can be done by allowing periodic repetitions with period $p>1$ in the sequence of arguments U_j (the fixed point case corresponds to $p=1$). For instance, the sequence of arguments corresponding to some initial condition for which a periodic subsequence with period $p=2$ begins at the mth generation reads $U_0U_1\ldots U_{m-1}U_mU_{m+1}U_mU_{m+1},\ldots,$ where $U_m\neq U_{m+1}$ (modulo 2π). This again leads to the exponential growth of $|F_n|$, if there is an eigenvalue of the matrix $M(U_{m+1})M(U_m)$ with a modulus greater than one.[9]

In conclusion, the general expression of the scattering vector $q(p,m,k)$ given by Eq. (9) is derived by imposing to the map (15) the condition to produce a periodic sequence of arguments with period $p\geq 1$ starting with the mth generation. These values of q correspond to the location of diffraction peaks which eventually grow as powers of L_n if and only if, (i) at least one eigenvalue of the matrix $M_p=M(U_{m+p-1})\cdots M(U_{m+1})M(U_m)$ is greater than one in absolute value, and (ii) the Fourier transforms $f_A(q),f_B(q)$ are not zero.

The violation of one of the conditions (i) or (ii) above is equivalent to the quasiextinction of the peaks, that is, in these cases the scaling exponent α is zero. The violation of condition (ii) gives trivial extinctions at values of the scattering vectors $q=(2l\pi/a), l\neq 0$. The discussion of the condition (i) requires an investigation of the matrix M_p. An inspection of the values taken by the entries $m_{ij}(p)$ of M_p when $q=q(p,m,k)$ and $k\neq 0$ indicates that $m_{21}(p)=0$ and the eigenvalue $m_{22}(p)=1$ for any $p\geq 1$. This shows that, at variance with the case when $q=0$, the contribution $|B_n|$ of the gaps to the scattering amplitude ceases to grow with their length beginning with the mth generation, that is their influence in the spectrum is diminished. The contribution of the gaps with $n>m$ is furthermore reduced to zero if k is an integer multiple of s^p-1, when $B_{m+l}=0$ for any $l>0$.

The second eigenvalue $m_{11}(p)$ of M_p is a product of factors $S_r[2s^l 2k\pi/(s^p-1)]$, $l=0,1,\ldots,p-1$, and, therefore, is zero whenever $2rk$ is an integer multiple of s^p-1 and $2k$ is not. Then $|F_n|=|B_m|$ for any $n>m$, which implies $\alpha=0$. In this case the peaks are entirely due to the B component, but their intensities no longer grow with the thickness of the superlattice for generations greater than m.

When $p=1$ and k is a multiple of $r-1$ then $m_{11}(1)=r$ and $m_{12}(1)=(r-1)e^{-ik\pi/(r-1)}$. Then the condition (i) holds and Eq. (16) indicates that after some transient behavior up to the $(m-1)$th generation the peak begins to grow with L_n according to Eq. (10), with the scaling index given by Eq. (11). (The contribution of the transient regime to intensity is encoded in the coefficient C and its influence decreases with n.) Taking into account the fact that r is the maximum possible value of S_r and the values taken by U_j in a period p are by definition not equal (modulo 2π), it follows from Eq. (13) that the maximum value of the scattering exponent $\alpha(k,p)$ is only reached when $p=1$.

When $p=1$ and $r-1$ is not a divisor of k, there are two possible cases. The above discussed quasiextinctions ($S_r=0$) appear when rk is a multiple of $r-1$. Otherwise $m_{11}(1)=1$ and $m_{12}(1)=0$, and this represents a different type of quasiextinction, where $F_n=F_m$ for any $n>m$.

It is instructive to see how the features predicted by the general theory appear in the numerical simulations from Sec. IV and the diffractograms from Figs. 4 and 5. In the case of the triadic Cantor superlattice ($r=2$), all the peaks with maximum growth rate ($p=1$) and $m\leq n-1$ are seen in Fig. 6. The intensity extrema indexed with $p=2$ can be observed whenever they are not covered by the much stronger $p=1$ peaks. The only pre-

dicted quasiextinctions with $m=2$, which exist in the q range of Fig. 6, are for $k=34,38$. The intensities are indeed stationary at $q(2,2,34)$ and $q(2,2,38)$ when n grows, as expected. In Fig. 6 another set of quasiextincted peaks corresponding to $p=2$, $m=3$ and even k can be seen when $n \geq 5$. The instrumental broadening of the main $p=1$ peaks precludes the detection of the $p \geq 2$ extrema in the conventional diffractograms from Figs. 4 and 5. Nevertheless, the quasiextinction of the $p=1$ peaks with odd k predicted by the theory in the case $r=3$ can clearly be seen in Fig. 5. For 2θ values below 2° the quasiextincted peaks with odd k are visible but are, in general, less intense compared with the peaks with even k values. This explains why the (1,0,1) peak is dominated by the (1,2,24) peak as mentioned in Sec. III. At higher 2θ values, the peaks with odd k values are not observed.

In what follows we briefly discuss the nature of the spectra in the thermodynamic limit. The Fourier transform of the Cantor superlattice can be split in a contribution B_n coming from the B system plus a term proportional to the Fourier transform F_n^A of the distribution of A layers as follows:

$$F_n = \left[1-\frac{f_B}{f_A}\right] F_n^A + B_n \ , \tag{17}$$

where $F_n^A(q)=\prod_{j=0}^{n-1} S_r(2qs^j)$. As discussed above, the only peaks the B system generates in the large n limit are the δ peak at $q=(2\pi/a)$ and the quasiextincted peaks corresponding to $S_r=0$. Therefore the main information regarding the fine peak structure of the Fourier spectrum is encoded in F_n^A. This allows us to formally neglect the B component by taking its scattering power zero. (As a secondary consequence all the quasiextinct peaks with $S_r=0$ will really become extinct, but this does not significantly change the aspect of the spectra for large n.) Then $H(2\pi/a)$ becomes strictly subunitary and the integrated intensity as defined by Eq. (2) loses its meaning of a *normalized* intensity distribution. This happens because the component A (which is responsible for the self-similar structure in diffractograms) occupies a fraction of the total thickness of the system that becomes negligible in the thermodynamic limit, and thus the peaks grow too slow with L to ensure normalization. Consequently, the intensity measure μ is irrelevant for the description of the fine spectrum. Nevertheless, physically relevant quantities can be defined by normalizing the intensity to the total thickness of the layers of type A. The renormalized scattering amplitudes read

$$R_n^{(r)}(q)=\frac{I_{L_n}(q)}{ar^n} \ , \tag{18}$$

and are known as generalized Riesz products.[17] The spectra are then described by functions analogous to the integrated intensity, which read

$$h_r(q)=\lim_{n\to\infty}\int_0^q R_n^{(r)}(q')dq' \ . \tag{19}$$

In the infinite n limit the Riesz products generate positive measures ρ_r, which act on sets of points in the reciprocal space. These measures are defined similarly to the intensity measure by

$$h_r(q)=\int_0^q d\rho_r(q') \ . \tag{20}$$

It can be shown that ρ_r are probability measures[17] [i.e., $\int_0^{2\pi/a} d\rho_r(q)=1$], and moreover that ρ_2 is purely singular continuous.[29] *According, with growing n the self-similar parts of the (appropriately normalized) spectra of the triadic Cantor superlattice reflect, with increasing precision, the main features of a singular continuous measure.* Extrapolating this result, we can expect that the similar generation of peaks observed in the cases with $r>2$ is associated again to SC measures, but a proof of this conjecture remains to be derived.

VI. DETAILED DIFFRACTION ANALYSIS

A detailed analysis of the spectra was performed in order to confirm the theoretical results. To accurately predict the position of the peaks, Eq. (9) had to be corrected to take into account the deviation of the refractive index η, from unity.[30] Then the peak positions in 2θ are given by

$$2a\sin(\theta)\left[1+\frac{\eta^2-1}{\sin^2(\theta)}\right]^{1/2}=\frac{k}{s^m(s^p-1)}\lambda \ , \tag{21}$$

where λ is the wavelength of the x-ray radiation. The values of a and η were achieved by linearizing Eq. (21).[31] To resolve the $p=1$ peaks with $m=4$ and 5, which cannot be seen in the low-resolution measurement presented in Fig. 4, a detailed x-ray-diffraction scan was conducted on the same sample in a smaller-angle region. Detailed measurements were also made for the 5th generation of the Cantor middle third superlattice ($r=2$) with nominally $a=1.55$ nm. The detailed diffractograms from the 5th and 6th generations of the Cantor middle third superlattices are reproduced in Figs. 8 and 9, respectively. In Fig. 8, all the $p=1$ peaks with $m \leq 4$ and some $p=2$ peaks are resolved. Also included in Fig. 8 is a dynami-

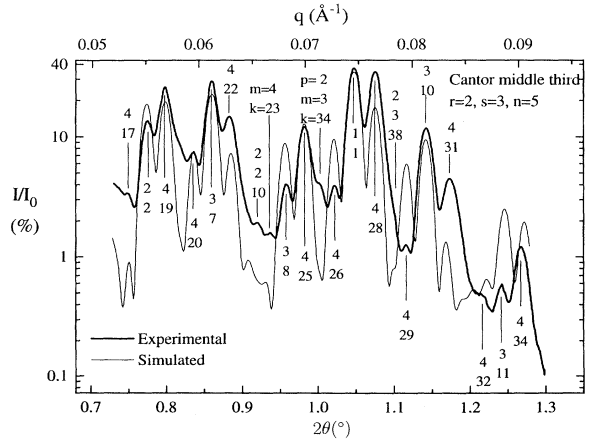

FIG. 8. Diffractogram from a detailed θ-2θ XRD measurement on the fifth generation of the Cantor middle third superlattice ($r=2$). The a-Ge and a-Si layer thicknesses were nominally $a=1.55$ nm. The 243 ($s^n=3^5$) A and B layers in the Cantor structure results in a total nominal thickness of 376.6 nm. A numerical simulation is also included.

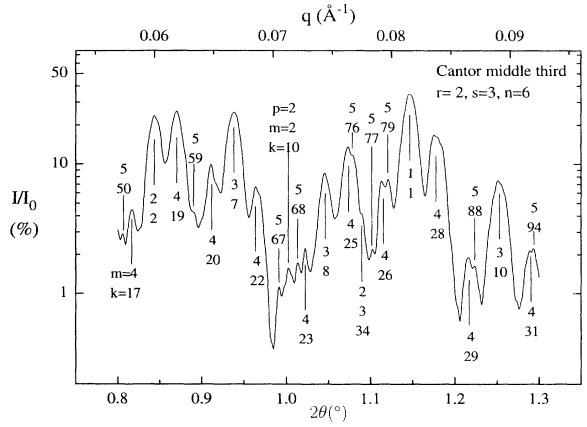

FIG. 9. Diffractogram from a detailed θ-2θ XRD measurement on the sixth generation of the Cantor middle third superlattice ($r=2$). The a-Ge and a-Si layer thicknesses were nominally $a=1.4$ nm. The 729 $s^n=3^6$) A and B layers in the Cantor structure results in a total nominal thickness of 1020.6 nm.

cal calculation from a Cantor profile with the same thicknesses as the measured superlattice. The simulation curve fits the measured curve very well regarding peak positions and a similar structure of peak intensities can be seen. The fit could probably be improved with a better model of the interfaces in the film. In Fig. 9 all the $p=1$ peaks seen in Fig. 8 can be observed. Since the measurement is made on a superlattice grown to the 6th generation, $p=1$ peaks with $m=5$ are present. The most pronounced of these peaks are indexed in Fig. 9.

Another detailed diffractogram, obtained from the same sample as presented in Fig. 5, is shown in Fig. 10. Peaks with $m=3$ are resolved in between the peaks with $m\leq 2$, as predicted by theory. The quasiextinction of odd $p=1$ peaks, already seen in Fig. 5, is obvious in Fig. 10, where the only detected odd peaks are (1,3,45) and (1,3,55).

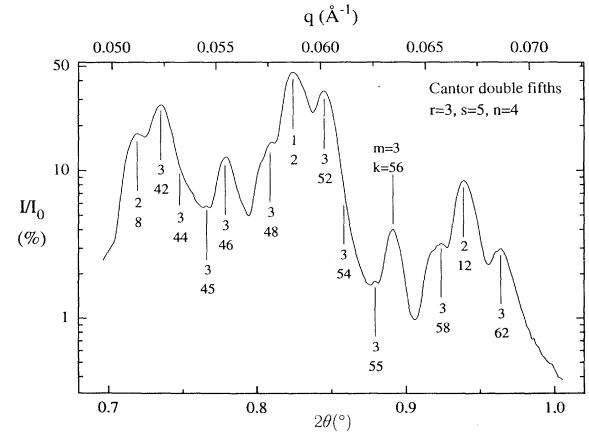

FIG. 10. Diffractogram from a detailed θ-2θ measurement on the fourth generation of the Cantor double fifths superlattice ($r=3$). The a-Ge and a-Si layer thicknesses were nominally $a=1.4$ nm. The 625 ($s^n=5^4$) A and B layers in the Cantor structure results in a total nominal thickness of 875 nm.

Although the amorphous superlattices are of good quality with well defined layers, they contain imperfections such as small layer thickness fluctuations and some interface mixing. In Sec. IV it was shown that such imperfections mainly influences the peak intensity, whereas the relative peak positions are much less affected. Therefore the difference between the intensities in the numerical calculation and measurement in Fig. 8 is expected since a perfect structure with ideally sharp interfaces was used in the model. However, the general features regarding the peak intensities mentioned in previous sections can be seen. For instance, the fact that peaks with smaller m should be more intense than neighboring peaks with higher m values is in general true. This simplifies the procedure of indexing the numerous peaks in the Cantor diffractograms.

When comparing the diffractograms with the analytical expressions and numerical calculations, a very good agreement regarding peaks positions is found. The a values achieved from the linearizations differed with less than 3% from the nominal values. The refractive index values were found to deviate from unity with approximately 1×10^{-5}. For the detailed scans, the measured and predicted 2θ peak positions deviated with a maximum of 1.1%.

VII. CONCLUSIONS

In this work, the x-ray diffraction from superlattices modulated according to Cantor sets was investigated both theoretically and experimentally. Expressions for the positions of the diffraction peaks and scaling laws for intensities were analytically derived. Accordingly, the peaks were indexed by three integers and the largest scaling exponents were found to be proportional to the fractal dimensions of the associated Cantor sets.

The theoretically derived position of the peaks were in a very good agreement with the results of the diffraction experiments and numerical calculations. However, numerical simulations showed that the scaling laws predicted by theory for perfect Cantor superlattices are actually strongly affected by absorption and imperfections in more realistic sample models.

A theoretical investigation of the nature of the diffraction spectra in the thermodynamic limit revealed some aspects which are specific to the fractal systems. It was shown that a correct global description of the self-similar part of the spectra can be achieved if the diffracted intensity is normalized to the total thickness of the layers representing the minoritary component in the superlattices. This is at variance with the full system size normalization previously used for the characterization of the spectra of nonfractal systems. The correctly normalized intensities of the Cantor superlattices were shown to be described in the large system limit by generalized Riesz products. Moreover, the spectral measure associated to the self-similar part of the diffraction pattern of the perfect triadic Cantor superlattice was found to be singular continuous.

We believe the above results could stimulate the interest in the structural investigation of fractal superlattices and the characterization of the measures which

govern the distribution of the intensity maxima in their spectra. In particular, it would be interesting to study to what extent these measures can be used to qualitatively distinguish between spectra of fractals with various degrees of complexity, in a similar way as the intensity measure is used in the characterization of the degree of order for nonfractal systems.

ACKNOWLEDGMENTS

The Swedish Research Council for Engineering Sciences (TRF) is acknowledged for financial support. M.D. thanks P. Gartner for useful discussions and the Department of Physics at Linköping University for financial support.

---

*On leave from Institute of Physics and Technology of Materials, R-76900, Bucharest-Magurele, Romania.

[1]D. Shechtman, I. Blech, D. Gratias, and J. W. Cahn, Phys. Rev. Lett. **53**, 1951 (1984).

[2]W. Schmidt, J. Appl. Cryst. **24**, 414 (1991).

[3]R. Merlin, K. Bajema, R. Clarke, F.-Y. Juang, and P. K. Bhattacharaya, Phys. Rev. Lett. **55**, 1768 (1985); J. Birch, M. Severin, U. Wahlstrom, Y. Yamamoto, G. Radnoczi, R. Riklund, J.-E. Sundgren, and L. R. Wallenberg, Phys. Rev. B **41**, 10 398 (1990).

[4]R. Merlin, K. Bajema, J. Nagle, and K. Ploog, J. Phys. (Paris) Colloq. **48**, C5-503 (1987).

[5]F. Axel and H. Terauchi, Phys. Rev. Lett. **66**, 2223 (1991); M. Kolář, *ibid.* **73**, 1307 (1994); F. Axel and H. Terauchi, *ibid.* **73**, 1308 (1994).

[6]*Quasicrystals, Networks, and Molecules of Fivefold Symmetry,* edited by I. Hargittai (VCH, New York, 1990).

[7]Aubry, C. Godreche, and J. M. Luck, Europhys. Lett. **4**, 693 (1987); C. Godreche and J. M. Luck, J. Phys. A **23**, 3769 (1990); Phys. Rev. B **45**, 176 (1992); J. M. Luck, C. Godreche, A. Janner, and T. Janssen, J. Phys. A **26**, 1951 (1993).

[8]M. Severin, J. Phys. Condens. Matter **1**, 6771 (1989).

[9]Z. Cheng and R. Savit, J. Stat. Phys. **60**, 383 (1990); M. Kolar, B. Iochum, and L. Raymond, J. Phys. A **26**, 7343 (1993); M. Kolar, Phys. Rev. B **47**, 5489 (1993).

[10]C. Allain and M. Cloitre, Phys. Rev. B **33**, 3566 (1986); D. L. Jaggard and X. Sun, Opt. Lett. **15**, 1428 (1990); T. J. Cui and C. M. Liang, J. Phys. D **26**, 1843 (1993).

[11]G. Chen and W. Ziqin, Solid State Commun. **76**, 269 (1990).

[12]F. Axel, J. P. Allouche, and Z.-Y. Wen, J. Phys. Condens. Matter **4**, 8713 (1992).

[13]Z. Cheng, R. Savit, and R. Merlin, Phys. Rev. B **37**, 4375 (1988).

[14]The integrated intensity is here defined in analogy with the integrated density of states used in the characterization of the electronic spectra. See also Ref. 7.

[15]W. Rudin, *Real and Complex Analysis* (McGraw-Hill, New York, 1974).

[16]K. Mahler, J. Math. Phys. **6**, 158 (1927).

[17]M. Queffelec, in *Substitution Dynamical Systems,* Lecture Notes in Mathematics Vol. 1294 (Springer Verlag, Berlin, 1987).

[18]M. Kohmoto and Y. Oono, Phys. Lett. **102A**, 145 (1984); S. Ostlund and R. Pandit, Phys. Rev. B **29**, 1394 (1984); J.-M. Luck, *ibid.* **39**, 5834 (1989).

[19]B. B. Mandelbrot, *The Fractal Geometry of Nature* (Freeman, San Francisco, 1982).

[20]K. Järrendahl, B. Pecz, J.-E. Sundgren, and H. Arwin, Thin Solid Films **240**, 7 (1994).

[21]K. Järrendahl, J. Birch, M. Dulea, H. Arwin, and J.-E. Sundgren, Thin Solid Films **246**, 120 (1994).

[22]K. Järrendahl, J. Birch, L. Hultman, L. R. Wallenberg, G. Radnoczi, H. Arwin, and J.-E. Sundgren, in *Amorphous Silicon Technology—1992,* edited by M. J. Thompson, Y. Hamakawa, P. G. LeComber, A. Madan, and E. A. Schiff, MRS Symposia Proceedings No. 258 (Materials Research Society, Pittsburgh, 1992), p. 535.

[23]K. Järrendahl, G. Radnoczi, Zs. Czigany, J. Birch, and J.-E. Sundgren (unpublished).

[24]D. K. G. de Boer, Phys. Rev. B **44**, 498 (1991).

[25]L. G. Parrat, Phys. Rev. **95**, 359 (1954).

[26]S. K. Sinha, E. B. Sirota, S. Garnoff, and H. B. Stanley, Phys. Rev. B **38**, 2297 (1988).

[27]S. K. Sinha, Physica B **173**, 25 (1991).

[28]J. M. Cowley, *Diffraction Physics* (North-Holland, Amsterdam, 1975); E. Spiller, Rev. Phys. Appl. **23**, 1687 (1988).

[29]A. Zygmund, *Trigonometric Series* (Cambridge University, Cambridge, England, 1968), Vol. I.

[30]B. K. Agarwal, *X-Ray Spectroscopy, an Introduction* (Springer, Verlag, Berlin, 1979).

[31]V. Dupuis, M. F. Ravet, C. Téte, M. Piecuch, and B. Vidal, J. Appl. Phys. **68**, 3348 (1990).

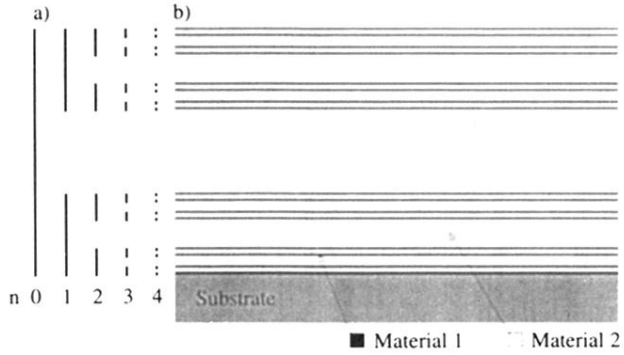

FIG. 1. (a) The first four generations leading to the Cantor middle third set ($r=2$). (b) A schematic drawing of a Cantor superlattice built according to the fourth generation of the Cantor middle third structure. The gaps and segments are represented by two different materials.

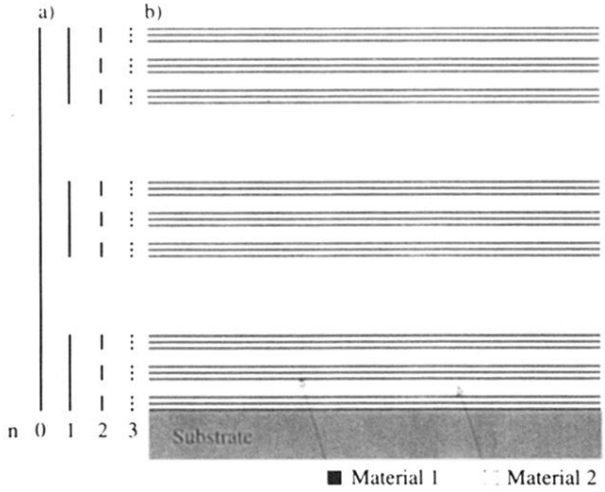

FIG. 2. (a) The first three generations leading to the Cantor double fifths set ($r=3$). (b) A schematic drawing of a Cantor superlattice built according to the third generation of the Cantor double fifths structure. The gaps and segments are represented by two different materials.

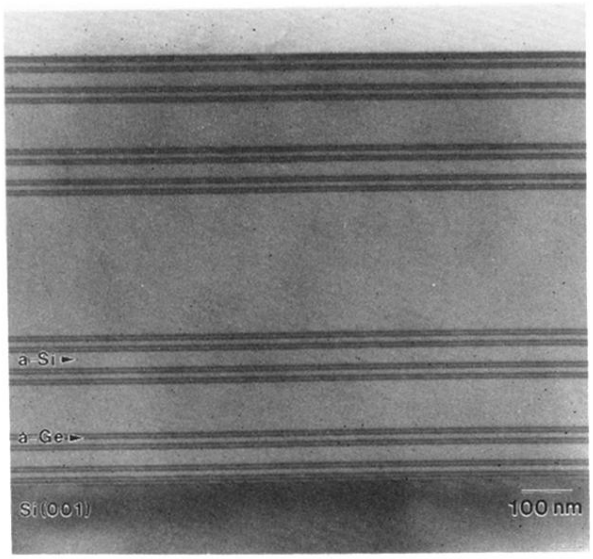

FIG. 3. An XTEM micrograph of the sixth generation of a Cantor middle third superlattice ($r=2$). The segments and gaps are represented here by layers of *a*-Ge and *a*-Si, respectively. In the image only the first five generations are resolved.